Generation of the neutron response function of an NE213 scintillator for fusion applications

EUROFUSION WPJET1-PR(16) 16127

F Binda et al.

Generation of the neutron response function of NE213 scintillators for fusion applications

Preprint of Paper to be submitted for publication in
Nuclear Instruments and Methods in Physics Research
Section A

This work has been carried out within the framework of the EUROfusion Consortium and has received funding from the Euratom research and training programme 2014-2018 under grant agreement No 633053. The views and opinions expressed herein do not necessarily reflect those of the European Commission.

Generation of the neutron response function of NE213 scintillators for fusion applications

F. Binda[a,*], J. Eriksson[a], G. Ericsson[a], C. Hellesen[a], S. Conroy[a], M. Nocente[b,c], E. Andersson Sundén[a], JET Contributors[d,1]

[a] *Department of Physics and Astronomy, Uppsala University, Uppsala, Sweden*
[b] *Dipartimento di Fisica "G. Occhialini", Università degli Studi di Milano-Bicocca, Milano, Italy*
[c] *Istituto di Fisica del Plasma "P. Caldirola", Milano, Italy*
[d] *EUROfusion Consortium, JET, Culham Science Centre, Abingdon, OX14 3DB, UK*

Abstract

In this work we present a method to evaluate the neutron response function of a NE213 liquid scintillator. This method is particularly useful when the proton light yield function of the detector has not been measured, since it is based on a proton light yield function taken from literature, MCNPX simulations, measurements of gamma-rays from a source and measurements of neutrons from fusion experiments with ohmic plasmas. The inclusion of the latter improves the description the proton light yield function in the energy range of interest (around 2.46 MeV).

We apply this method to a NE213 detector installed at JET, inside the radiation shielding of the magnetic proton recoil (MPR) spectrometer, and present the results from the calibration along with some examples of application of the response function to perform neutron emission spectroscopy (NES) of fusion plasmas.

We also investigate how the choice of the proton light yield function affects the NES analysis, finding that the result does not change significantly. This points to the fact that the method for the evaluation of the neutron response

*Corresponding author
Email address: federico.binda@physics.uu.se (F. Binda)

[1] See the Appendix of F. Romanelli et al., Proceedings of the 25th IAEA Fusion Energy Conference 2014, Saint Petersburg, Russia.

function is robust and gives reliable results.

Keywords:
NE213 scintillator; Neutron spectroscopy; response function; proton light yield;

1. Introduction

Neutron emission spectroscopy (NES) can provide valuable information about a fusion plasma based on the emission of 2.5 MeV and 14 MeV neutrons from the d+d and d+t reactions respectively [1, 2, 3]. Plasma parameters such as fuel ion ratio [4], thermal emission fraction [5], and many others can be measured by means of NES analysis. Compact neutron detectors such as NE213 liquid scintillators are regularly employed as neutron counters and in neutron cameras, but they have not been used much for NES analysis, since their energy resolution is poor and their response to neutrons is far from optimal for spectroscopy. Nevertheless, they have the potential to provide profile information of the above-mentioned fusion plasma parameters through NES analysis. Some attempts to obtain plasma parameters with NE213 detectors has been presented in

In this work we present a method to calculate a reliable neutron response function of NE213 detectors. The neutron response function can then be used to perform NES analysis, after applying the following integral transform:

$$M(ch) = \int R(ch, E_n) S(E_n) \mathrm{d}E_n, \tag{1}$$

where S is a neutron spectrum, R is the response function, M is the measurement, ch is the measured quantity (total integrated charge for NE213 detectors) and E_n is the neutron energy.

Some of the neutrons and gamma-rays that reach the detector transfer part of their energy to protons and electrons respectively. The neutrons interact mostly through elastic scattering, while the gammas through Compton scattering [6]. Since in both cases the recoil particle is charged, it induces the emission of scintillation light in the detector, with an intensity that depends on the energy

and type of the particle. The distribution of the intensity of the light emission from the recorded events is referred to as the pulse height spectrum (PHS). The experimental PHS is obtained from the integration of the voltage values of the individual scintillator pulses (total charge of the pulses) and it is initially expressed in arbitrary units. The actual light emission values, usually expressed in units of eVee (electronvolt electron equivalent), can be obtained only after a proper calibration has been performed.

The light output from the NE213 that results from the interaction of neutrons in the scintillator is related to the neutron energy through the detector's neutron response function. Therefore obtaining the response of the detector to neutrons and gammas is a crucial step towards performing neutron spectroscopy analysis. In particular, the relationship between the neutron energy and the corresponding maximum light output is not linear and it is referred to as the proton light yield (output) function. In previous works either the response function [7] or the proton light yield function [8, 9] was measured at an accelerator facility. This is good practice, but sometimes it can be inconvenient or impossible to perform the measurements. Furthermore, it is important to notice that once the detector is moved to another facility, the response may change due to changes in cables, background noise, acquisition system, deterioration of the photomultiplier tube (PMT) etc. All these changes can introduce differences in the resolution and in the response of the detector. Also the light output might vary over time because of deterioration of the scintillation material. Thus, even in cases when a calibration has been obtained prior to the installation at the fusion device, monitoring and adjustment will be required in situ.

The neutron response calculation method presented here is based on MCNPX [10] simulations, a standard proton light yield function from literature and measured data from a gamma source and from fusion experiments with ohmic plasmas. This procedure means that the detector is calibrated and characterized in-situ in its final measurement position. Specifically, the use of ohmic plasma discharges as a calibration source allows to adjust the proton light yield function to the exact experimental set-up that is used in later measurements where the

NES analysis is performed to obtain physics results.

In section 2 we describe the experimental set-up, the data processing, and the method for the calculation of the response of the detector; in section 3 we briefly discuss the modeling of the neutron emission; in section 4) we show the results of the calibration and of the NES analysis of data collected during JET experiments; finally we discuss the results in section 5.

2. Materials and methods

2.1. Detector Installation

The NE213 detector used in this study is installed inside the radiation shielding of the Magnetic Proton Recoil (MPRu) neutron spectrometer [11] at the JET fusion experimental facility, UK. The NE213 is positioned in front of the MPRu beam dump, and the two instruments share the same tangential line of sight through the plasma. The distance from the NE213 to the plasma center is about 11 m. The NE213 active volume is a cylinder with 12.3 mm diameter and 8.4 mm thickness. The scintillation light is detected by a Hamamatsu R5611 [12] PMT. The PMT electrical pulses are transmitted through about 90 m of low loss coaxial cable to the data acquisition equipment. The PMT voltage pulses are digitized by an SP Devices ADQ214 [13] digitizer (14 bit, 400 MSPS) and the full pulse shapes are stored on a local computer for a later offline analysis. The detector is equipped with a ^{22}Na gamma source that provides an absolute reference for calibration and monitoring of the PMT gain. An LED pulse generator is connected to the PMT through a light fibre and it is used to monitor short term gain drifts of the PMT.

2.2. Data processing

Converting the raw data to the PHS requires a few steps. First of all a general voltage offset (baseline level) needs to be subtracted from the pulses. Then the pulses are integrated by summing the sample values in two different time ranges, a short and a long range, as shown in Figure 1.

We use two ranges of integration in order to perform pulse shape discrimination (PSD) between pulses induced by gamma rays and pulses induced by neutrons. The total integrated charge is just the sum of the short and long charge ($Q_{tot} = Q_{short} + Q_{long}$), while the PSD factor is given by:

$$PSD = \frac{Q_{long}}{Q_{tot}}. \tag{2}$$

The events can then be displayed in a 2D plot, with Q_{tot} on the x axis and PSD on the y axis. One can then apply cuts to select the regions containing gamma, neutron and pile-up events, as shown in Figure 2. For the counting rates that were measured with the detector in the present study, this method is sufficient to get rid of most pile-up events.

2.3. Response function generation

The response function of the detector to gamma and neutron irradiation is estimated from a combination of MCNPX simulations and measurements. The simulations are used to calculate the shape of the response of the detector to monoenergetic gamma and neutron interactions. However the simulations do not include the energy resolution of the detector or the conversion between total charge (pulse height spectrum "channel") and light yield, i.e. the energy cali-

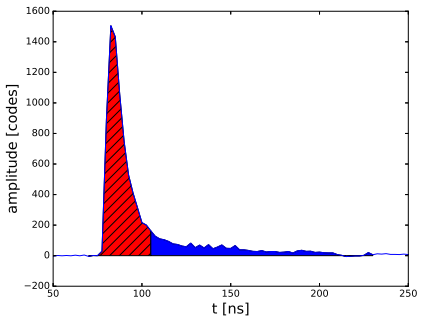

Figure 1: Example of scintillator pulse recorded with the NE213 detector, after the baseline restoration has been performed. The colored areas show the short charge (red with black lines) and long charge (blue).

bration. These effects need to be parametrized and the parameters estimated by comparison with measurements. The resolution is modeled as a three-parameter formula [14]:

$$R(E) = \frac{FWHM(E)}{E} = \sqrt{\alpha^2 + \frac{\beta^2}{E} + \frac{\gamma^2}{E^2}}, \tag{3}$$

where α, β and γ are the parameters and E is the energy.

The energy calibration is described by the linear relationship:

$$E[keVee] = k \cdot ch + m, \tag{4}$$

where ch represents the total charge value and E is the detector light output, expressed in keVee.

In the case of gamma interactions, the light output (in keVee) is directly proportional to the energy deposited by the recoil electron (in keV). In contrast the light output of recoil protons from neutron interactions cannot be described by a linear relationship with the deposited proton energy, and it is usually described by a 3rd or higher degree polynomial, with different coefficients for different energy intervals. The method we developed here allows to obtain reliable results even when the proton light yield function has not been measured. We start from a light yield function taken from literature and we adapt this

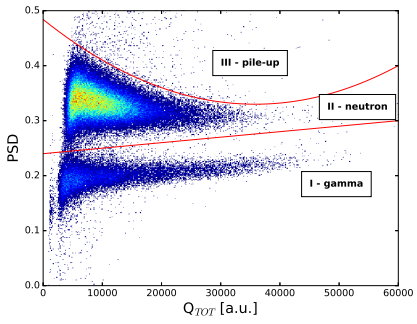

Figure 2: PSD vs total charge plot for JET discharge 86459. The red lines show the cuts applied to select the gamma, neutron and pile-up region.

assumption to our detector by introducing a further calibration parameter, λ, which acts on the proton light yield as a multiplication factor:

$$L'_p = \lambda \cdot L_p, \tag{5}$$

where L'_p is the calibrated proton light yield function, while L_p is the one from literature.

To estimate the impact of this assumption on the NES analysis, we calculated three separate response functions, using three different light yield function. We then compared the results obtained with each of them to have an indication of the sensitivity of the results on this choice. Figure 3 shows the light yield functions that we used. Two of them are taken from publications ("Hawkes" [15] and "'Verbinski" [16]), one ("ED") is taken from the database of the simulation code NRESP [17].

Since the calibration is based on data that consists mostly of neutrons of energies near 2.46 MeV, the agreement between the three functions is largely improved around this value. However relatively large differences remain at higher energies.

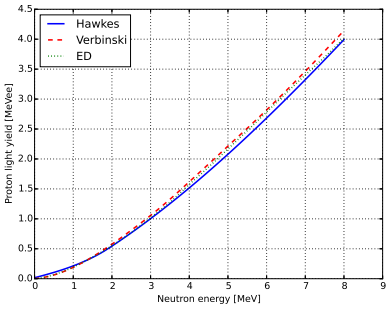

Figure 3: Proton light yield functions used for the simulation of the neutron response.

The measurements used to estimate the response parameters (α, β, γ, k, m, λ) are: i) gamma-rays from a ^{22}Na source permanently installed in front of the detector, which emits monoenergetic gammas at 1275 and 511 keV, and ii) the neutron PHS accumulated during the ohmic phase of about 650 JET plasma

discharges. The latter provides us with information about the proton light yield function, allowing us to estimate the calibration parameter λ. This would not be possible with the sodium source.

To describe the gamma data we only simulate the two energies of interest, while for the neutron data we produce a response matrix built from MCNPX simulations of the response of the detector to monoenergetic neutrons of different energies (from 1 to 20 MeV in 50 keV steps). The comparison with measurements is performed after folding the response with Gaussian distributions with a spread that follows the resolution function of equation 3 and after calibrating it according to equation 4. The neutron response function is further calibrated according to equation 5.

3. Neutron spectra model

An estimate of the neutron spectrum at the detector position is obtained from Monte Carlo calculations [18] [19]. The starting point for these calculations is the velocity distribution of the ions in the plasma, which needs to be modeled. The ion velocity distribution model depends on the heating scheme and the plasma parameters. In this work we analyzed data collected from plasmas heated with three different heating schemes: ohmic heating (used for calibration of the detector response), neutral beam injection (NBI) heating, and NBI + ion cyclotron resonance heating (ICRH).

The ohmic neutron spectrum is very well known, therefore we use it as a known source for the calibration of the response. It is well described by a Gaussian distribution [20] whose parameters depend on the plasma ion temperature. At JET the temperature of ohmic plasmas is about 2 keV [21], which results in a Gaussian centered at about 2.46 MeV, with full width half maximum (FWHM) of about 117 keV.

For plasmas with NBI heating only the ion velocity distribution is calculated using the TRANSP code, a simulation tool widely used in fusion research [22].

For the more complex heating scheme which uses a combination of NBI

and ICRH, the modeling is more complicated. We chose to analyze discharges where the ICRH was tuned on the 3rd harmonic of the deuterium ion cyclotron frequency, because this heating scheme produces highly energetic D fuel ions (up to a few MeV) whose energy is reflected in the emitted neutron spectrum as a high energy tail of considerable intensity. In this case the ion distribution is obtained using a previously developed 1D Fokker-Planck model [23, 24]. The two main parameters in the model are connected to the intensity and the endpoint (cut-off) energy of the ICRH-induced fast ion tail. For the analysis performed here, these two parameters were fixed from a fit to data collected with the TOFOR neutron spectrometer for the studied JET discharges [25]. We also here note that this model contained an assumption that the ICRH-induced fast ions will have pitch angles (the angle between the velocity of the ion and the magnetic field) evenly distributed in the range 80-100 degrees. A more detailed discussion about the assumptions of this model have been presented in [26] and will not be part of the discussion in this paper.

In all of these cases, a fraction of the neutrons that reach the detector have undergone scattering against the tokamak structures. We call these "backscattered" neutrons, and we include this effect in the neutron spectrum model by having a backscatter component calculated with MCNP [27].

Furthermore, in the NBI + ICRH case, we include also a triton burn-up neutron (TBN) component in the neutron spectrum. TBNs are produced from DT reactions ($D + T \rightarrow \alpha + n$) that occur in pure DD plasmas because the reaction $D + D \rightarrow p + t$ produces tritons, which in turn can interact with the D in the plasma. Even though the TBN emission is a small fraction (about 1%) of the total emission, it is relevant because it affects the end-point of the PHS tail, where the counting statistics is low. This end-point is particularly important in the NBI + ICRH scenario, therefore the inclusion of a TBN component is necessary for the correct description of the data.

4. Results

Examples of the NE213 pulse height spectra produced by the three different heating schemes that we analyzed are shown in Figure 4.

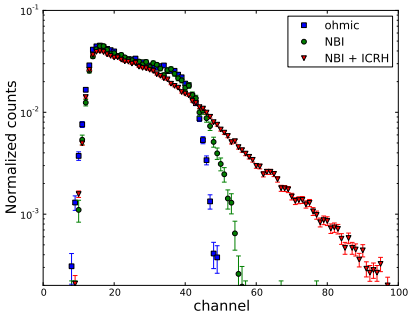

Figure 4: NE213 normalized pulse height spectra for JET discharges with ohmic heating (blue squares), NBI heating (green circles) and NBI + ICRH (red triangles).

As mentioned before, we use the ohmic data to calibrate the neutron response function. We then analyze NBI heated data because, besides the ohmic data, they are the simplest to model. Finally we analyze the more complicated case with ICRH, where the fast ion distribution is not as well known as in the case with NBI only.

4.1. Calibration

The result of the sodium spectrum fit is shown in Figure 5. Since the scintillation cell of the detector is small, we assume $\alpha = 0$ (in equation 3 α is related to volume effects). From this fit we obtain β, γ, k and m. The normalization factor of the two gamma components (511 keV and 1275 keV) are also free parameters of the fit.

The result of the fit to ohmic-heating neutron data is shown in Figure 6. From this fit we obtain λ. Also in this case the normalization factor of the two components is a free parameter.

Some example values of the calibration parameters obtained from the fits are shown in Table 1. These values can change over time and therefore they are

continuously monitored.

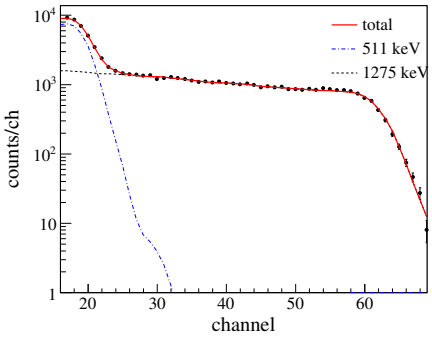

Figure 5: Experimental pulse height spectrum of the data from the ^{22}Na gamma source (points). The blue dash-dotted and the black dashed lines are the MCNPX responses of the detector to the two gamma energies (511 keV and 1275 keV respectively) after convolution with the resolution function. The bold red line is the sum of the two.

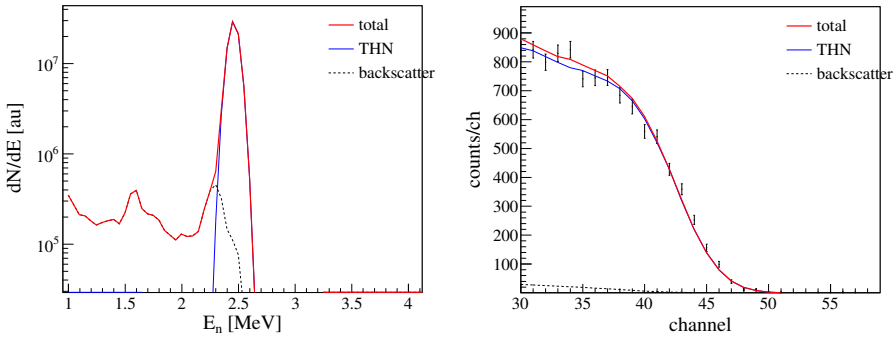

Figure 6: Left panel: neutron energy spectrum components used in the fit. Right panel: experimental neutron pulse height spectrum (sum over about 650 ohmic discharges) with the fitted components. The blue solid line is the thermal component, the black dashed line is the backscatter component, the red bold line is the sum of the two.

4.2. NBI heated discharges

As a first step of validation of the method we chose to analyze plasma discharges where the neutron emission is dominated by beam-thermal interactions, following what was done with the TOFOR spectrometer in [28]. This type of

Parameter	Value	Uncertainty	Units
k	16.939	0.010	keVee/ch
m	17.58	0.22	keVee
β	8.76	0.26	$\mathrm{MeVee}^{1/2}$
γ	4.53	0.20	MeVee
λ_H	0.967	0.02	-
λ_V	0.885	0.02	-
λ_E	0.930	0.02	-

Table 1: Example values of the calibration parameters resulting from the gamma and ohmic fits. The values of λ for the three light yield functions used are given ("Hawkes", "Verbinski", "ED").

discharges is the simplest to model, besides thermal plasmas which we already used for calibration purposes. We selected 5 suitable time intervals from 3 JET discharges (number 85227, 86996 and 86997). We observed that a satisfactory fit to the TOFOR data can be obtained using a beam-thermal component alone. Hence we concluded that beam-thermal interactions are the dominating source of neutrons in this scenario and we performed the analysis of the NE213 data with only such a component.

Figure 7 shows the neutron spectrum components and the experimental PHS for discharge 86997 with the fitted components. Since the fuel ion distribution, and hence the spectral shape of the neutron emission, was completely determined based on the TOFOR analysis, the only free parameter in this case is the normalization factor for the beam-thermal component. The normalization factor for the backscatter component was fixed from the total neutron yield measured by the fission chambers. It is worth noticing that, despite the PHS looking very similar to the ohmic one (Figure 6), it extends to higher integrated charge values. The difference between the two can be seen more clearly in Figure 4.

Table 2 shows the reduced Cash statistics values [29] obtained from the comparison of all the time intervals that we analyzed.

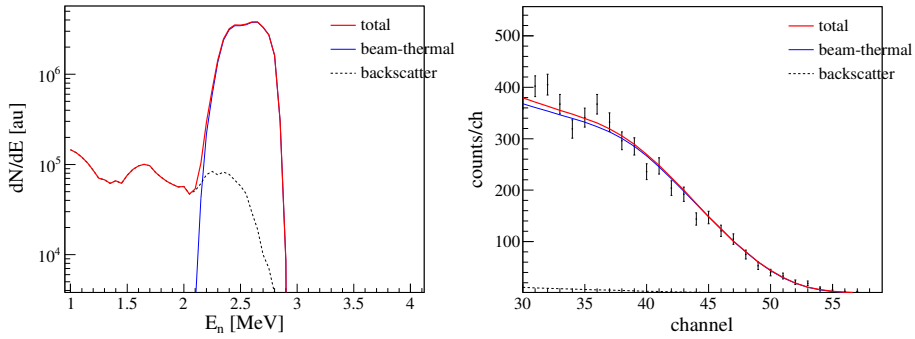

Figure 7: JET discharge number 86997. Left panel: neutron energy spectrum components used in the fit. Right panel: experimental neutron pulse height spectrum with the fitted components. The blue solid line is the beam-thermal component, the black dashed line is the backscatter component, the red bold line is the sum of the two.

Discharge number and time interval	**Reduced Cash statistics**
85227 9-14 s	1.91
85227 14-18 s	0.85
86996 7-13 s	1.14
86996 13-17.5 s	1.04
86997 7-17.5 s	1.29

Table 2: Reduced Cash statistics values obtained for JET discharges 85227, 86996 and 86997.

4.3. NBI + ICRH discharges

We compared the modeled and the measured PHS for three JET discharges: 86459, 86461 and 86464. As in the NBI heating only case, the normalization factor of the backscatter component is fixed from the total neutron yield measurement, while the normalization factors of the two direct components (NBI + ICRH and TBN) are free parameters.

We performed the comparison using the three response functions produced for the three proton light yield functions presented in section 2.3. We chose to do this using data from the 3rd harmonic ICRH experiment because in this case the neutron spectrum extends to high energies that go far beyond the energy

range of the ohmic discharges that we used to calibrate the light yield function.

The time intervals selected for the analysis were 10.5-12.1 s, 11-13 s and 11-13 s for the three discharges respectively.

Figure 8 shows the neutron spectrum components and the experimental PHS for discharge 86459 with the fitted components. Figure 9 shows instead a comparison of the results obtained using the three different proton light yield functions for the generation of the response function.

The comparison is performed using Cash statistics, and the results for all the discharges and light yield functions are presented in Table 3.

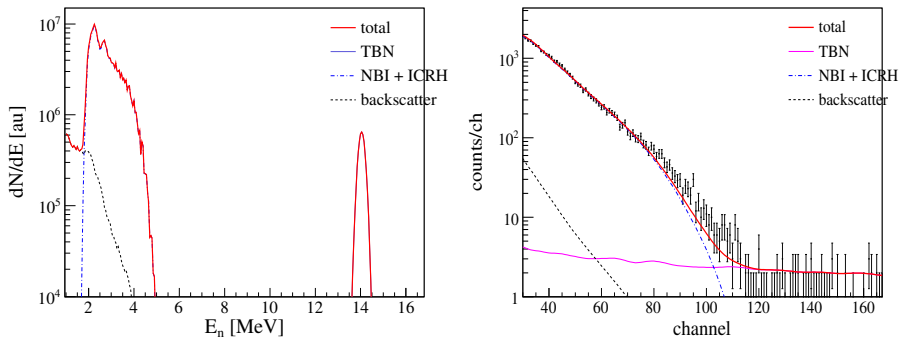

Figure 8: JET discharge number 86459. Left panel: neutron energy spectrum components used in the fit. Right panel: experimental neutron pulse height spectrum with the fitted components. The blue dash-dotted line is the NBI + ICRH component, the black dashed line is the backscatter component, the purple solid line is the TBN component and the red bold line is the sum of the three.

Discharge number	**Hawkes**	**ED**	**Verbinski**
86459	1.29	1.27	1.40
86461	1.38	1.27	1.21
86464	1.47	1.54	1.77
λ	0.967	0.885	0.930

Table 3: Reduced Cash statistics values obtained for JET discharges 86459, 86461 and 86464 using the three different response functions. The last line is a reminder of the values of the calibration parameter λ, which differs depending on the light yield function.

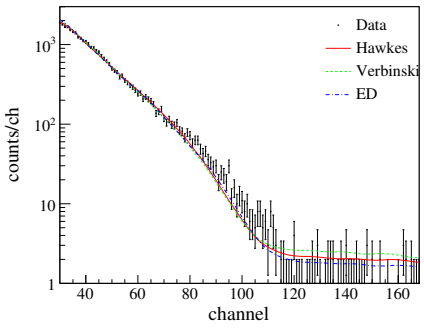

Figure 9: Comparison between the measured PHS for discharge 86459 and the model using the three different proton light yield functions. The lines are the sum of the different spectral components (backscatter, NBI + ICRH and TBN). Each line corresponds to a different proton light yield function.

5. Discussion and conclusions

In this work we have adopted a practical approach to the generation of a neutron response matrix for the used NE213 detector. We introduced a calibration parameter for the neutron response which we evaluated using experimental neutron data collected in the exact same conditions as the data that we later analyzed to obtain physics results. The introduction of this parameter makes the evaluation of the response robust, since the assumed proton light yield function is adjusted to better describe the system. The same procedure used in the calibration could be used even in cases where the neutron response or the proton light yield of the detector was measured at an accelerator, because changes of the experimental environment might affect the response (different cables, different noise levels etc.) and the proton light yield might change over time, for example due to deterioration of the scintillation material.

We analyzed the simple case of data from plasma discharges with NBI heating only. The neutron energy range is roughly the same as for ohmic plasmas, which were used to calibrate the response of the detector. The agreement between model and data was good, as shown by the Cash statistcs values obtained (Table 2).

The analysis of data from the NBI + ICRH heating experiments presented a more complex case. First of all, the ion velocity distribution is not as well known as in the NBI only case. Secondly, the neutron energies extend to high values, far from the energy range used in the calibration of the response of the detector. The comparison between model and experimental data gave good values of the Cash statistics (Table 3). However it can be noticed from Figure 8 that the model slightly underestimates the PHS in the total charge interval from 80 to 100. This slight discrepancy could be explained by some simplified assumptions made in the model. Indeed, it has been shown that modifications to these assumptions can result in a better fit. A more detailed discussion of this is outside the scope of this paper, but it has been presented in [26].

The use of different light yield functions for the response of the detector has a small effect on the results (see Table 3). The difference is small mostly due to the fact that the calibration factor λ reduces the differences between the light yield functions in the energy range near 2.46 MeV, which is the energy range of the majority of the neutron events in the analysed spectra. Furthermore, the inclusion of the λ parameter and its evaluation "on site" gives stability to the system, because of the possibility to monitor changes in the response.

We can then conclude that the method that we presented here for the evaluation of the neutron response function produces reliable results, and that the response function obtained can be applied to perform neutron emission spectroscopy of fusion plasmas. The method has indeed been applied to obtain physical results which were presented in [26] and [30].

6. Acknowledgments

This work has been carried out within the framework of the EUROfusion Consortium and has received funding from the Euratom research and training programme 2014-2018 under grant agreement No 633053. The views and opinions expressed herein do not necessarily reflect those of the European Commission.

References

[1] B. Wolle, Tokamak plasma diagnostics based on measured neutron signals, Physics Reports 312 (1999) 1–86. doi:10.1016/S0370-1573(98)00084-2.

[2] M. Tardocchi, et al., Diagnosis of physical parameters of fast particles in high power fusion plasmas with high resolution neutron and gamma-ray spectroscopy, Plasma Physics and Controlled Fusion 55 (2013) 074014. doi:10.1088/0741-3335/55/7/074014.

[3] C. Hellesen, et al., Measurements of fast ions and their interactions with MHD activity using neutron emission spectroscopy, Nuclear Fusion 50 (2010) 084006. doi:10.1088/0029-5515/50/8/084006.

[4] C. Hellesen, et al., Fuel ion ratio determination in NBI heated deuterium tritium fusion plasmas at JET using neutron emission spectrometry, Nuclear Fusion 55 (2) (2015) 023005. doi:10.1088/0029-5515/55/2/023005.

[5] C. Hellesen, et al., Neutron spectroscopy results of JET high-performance plasmas and extrapolations to DT performance, Review of Scientific Instruments 81 (2010) 10D337. doi:10.1063/1.3502326.

[6] G. F. Knoll, Radiation detection and measurement, John Wiley and Sons, Inc., 2000.

[7] F. Öhrn, et al., Compact NE213 neutron spectrometer with high energy resolution for fusion application, Nuclear Instruments and Methods in Physics Research A 592 (2008) 405–413. doi:10.1016/j.nima.2008.04.030.

[8] A. Zimbal, et al., Compact NE213 neutron spectrometer with high energy resolution for fusion applications, Review of Scientific Instruments 75 (2004) 3553–3555. doi:10.1063/1.1787935.

[9] M. Tajik, et al., Modeling NE213 scintillator response to neutrons using an MCNPX-PHOTRACK hybrid code, Nuclear Instruments and Methods in

Physics Research A 704 (2013) 104–110. doi:10.1016/j.nima.2012.12.001.

[10] See *http://mcnpx.lanl.gov/* for mcnpx code (accessed 26 april 2016).

[11] E. Andersson Sundén, et al., The thin-foil magnetic proton recoil neutron spectrometer MPRu at JET, Nuclear Instruments and Methods in Physics Research A 610 (2009) 682–699. doi:10.1016/j.nima.2009.09.025.

[12] See *http://www.hamamatsu.com/eu/en/product/category/3100/3001/r5611a/index.html* (accessed 26 april 2016).

[13] See *http://spdevices.com/index.php/adq214* (accessed 26 april 2016).

[14] G. Dietze, H. Klein, Gamma-calibration of NE 213 scintillation counters, Nuclear Instruments and Methods 193 (1982) 549–556. doi:10.1016/0029-554X(82)90249-X.

[15] N. P. Hawkes, et al., Measurements of the proton light output function of the organic liquid scintillator NE213 in several detectors, Nuclear Instruments and Methods in Physics Research A 476 (2002) 190–194. doi:10.1016/S0168-9002(01)01429-2.

[16] V. V. Verbinski, et al., Calibration of an organic scintillator for neutron spectrometry, Nuclear Instruments and Methods 65 (1968) 8–25. doi:10.1016/0029-554X(68)90003-7.

[17] G. Dietze, H. Klein, NRESP4 and NEFF4: Monte carlo codes for the calculation of neutron response functions and detection efficiencies for NE213 scintillation detectors, Tech. rep., PTB-ND-22, iSSN 0572-7170 (1982).

[18] L. Ballabio, Calculation and measurement of the neutron emission spectrum due to thermonuclear and higher-order reactions in tokamak plasmas, Ph.D. thesis, Uppsala University (2003).

[19] J. Eriksson, et al., Calculating fusion neutron energy spectra from arbitrary reactant distributions, Computer Physics Communications 199 (2016) 40–46. doi:10.1016/j.cpc.2015.10.010.

[20] H. Brysk, Fusion neutron energies and spectra, Plasma Physics 15 (1973) 611–617. doi:10.1088/0032-1028/15/7/001.

[21] B. Esposito, et al., Ohmic ion temperature and thermal diffusivity profiles from the JET neutron emission profile monitor, Plasma Physics and Controlled Fusion 35 (1993) 1433–1440. doi:10.1088/0741-3335/35/10/006.

[22] J. P. H. E. Ongena, et al., Numerical transport codes, Fusion Science and Technology 61 (2T).

[23] T. H. Stix, Fast-wave heating of a two-component plasma, Nuclear Fusion 15 (1975) 737–754. doi:10.1088/0029-5515/15/5/003.

[24] C. Hellesen, et al., Fast-ion distributions from third harmonic ICRF heating studied with neutron emission spectroscopy, Nuclear Fusion 53 (2013) –. doi:10.1088/0029-5515/53/11/113009.

[25] M. Gatu Johnson, et al., The 2.5-MeV neutron time-of-flight spectrometer TOFOR for experiments at JET, Nuclear Instruments and Methods in Physics Research A 591 (2008) 417–430. doi:10.1016/j.nima.2008.03.010.

[26] J. Eriksson, et al., Dual sightline measurements of MeV range deuterons with neutron and gamma-ray spectroscopy at JET, Nuclear Fusion 55 (12) (2015) 123026. doi:10.1088/0029-5515/55/12/123026.

[27] M. G. Johnson, et al., Modelling and TOFOR measurements of scattered neutrons at JET, Plasma Physics and Controlled Fusion 52 (8). doi:10.1088/0741-3335/52/8/085002.

[28] C. Hellesen, et al., Neutron spectroscopy measurements and modeling of neutral beam heating fast ion dynamics, Plasma Physics and Controlled Fusion 52 (8). doi:10.1088/0741-3335/52/8/085013.

[29] W. Cash, Parameter estimation in astronomy through application of the likelihood ratio, Astrophysical Journal 228 (1979) 939–947. doi:10.1086/156922.

[30] F. Binda, et al., Forward fitting of experimental data from a NE213 neutron detectorinstalled with the magnetic proton recoil upgraded spectrometer at JET, Review of Scientific Instruments 85 (2014) –. doi:10.1063/1.4895565.